Journal of Nuclear Materials 557 (2021) 153316

Contents lists available at ScienceDirect

Journal of Nuclear Materials

journal homepage: www.elsevier.com/locate/jnucmat

High radiation tolerance of an ultrastrong nanostructured NiCoCr alloy with stable dispersed nanooxides and fine grain structure

Chenyang Lu[a,b], Mingyang Li[c], Pengyuan Xiu[a], Xing Wang[d], Gihan Velişa[e,1], Li Jiang[a], Karren L. More[d], Jonathan D. Poplawsky[d], Yongqin Chang[c,*], Yanwen Zhang[e,f,*], Lumin Wang[a,g,*]

[a] Department of Nuclear Engineering and Radiological Sciences, University of Michigan, Ann Arbor, Michigan 48109, USA
[b] Department of Nuclear Science and Technology, Xi'an Jiaotong University, Xi'an, Shaanxi 710049, China
[c] School of Materials Science and Engineering, University of Science and Technology Beijing, Beijing 100083, China
[d] Center for Nanophase Materials Sciences, Oak Ridge National Laboratory, Oak Ridge, TN 37830, USA
[e] Materials Science and Technology Division, Oak Ridge National Laboratory, Oak Ridge, TN 37831, USA
[f] Department of Materials Science and Engineering, University of Tennessee, Knoxville 37996, USA
[g] Department of Materials Science and Engineering, University of Michigan, Ann Arbor, Michigan 48109, USA

ARTICLE INFO

Article history:
Received 25 May 2021
Revised 13 August 2021
Accepted 24 September 2021
Available online 25 September 2021

Keywords:
High entropy alloy
Irradiation effects
Mechanical alloying
Nanooxides
Atom probe
Tomography
NiCoCr

ABSTRACT

The present paper reports the irradiation behavior of nanostructured NiCoCr medium entropy alloy enhanced by Y-Hf-O nanooxides and fine grains produced by powder metallurgy. Ion beam irradiation to a peak dose of 130 dpa at 580°C produced neither detectable void swelling nor irradiation-induced hardening, in contrast to significant void swelling and property degradation of single phase NiCoCr concentrated solid-solution alloy under the similar irradiation condition. The dispersed nanooxides and high density of grain boundaries act as defect sinks that effectively annihilate irradiation-induced interstitials and vacancies. Furthermore, high-density nanooxides maintain their crystalline structures and stabilize the grain boundaries during irradiation.

1. Introduction

In the past decade, high entropy alloys (HEAs) and some medium entropy alloys (MEAs), two kinds of single-phase concentrated solid solution alloys (SP-CSAs) normally comprising multiple principal components, have generated substantial and persistence interests in the materials science community since they have been initially reported by Yeh [1]. This kind of CSAs possesses adjustable and multifunctional properties derived from the complex combination of compositional elements, such as high thermal stability and hardness, high strength-to-weight ratio, high-temperature strength, great wear and fatigue resistance, and significant corrosion resistance [2–6]. Recently, some HEAs, including FeNiMnCr [7], NiCoFeCrMn [8], NiCoFeCrPd [9,10], AlCoCrFeNi [11], and TiZrHfVMo [12], have been reported to possess many promising properties, including an excellent combination of strength and ductility, and a promising radiation-tolerant behavior. The enhanced radiation resistance has been attributed to the complex intrinsic transport properties of MEAs and HEAs, where the increased compositional complexity of CSAs can reduce the effective interstitial mobility and enhance the vacancy-interstitial recombination [8,9,13,14].

In our previous study, we found that increasing radiation resistance can be easily achieved by increasing the number of alloying elements in SP-CSAs [8]. However, recent work shows that increasing the number of component elements in SP-CSAs is not necessary to achieve outstanding mechanical properties. NiCoCr, a key member of SP-CSAs, exhibits a remarkable performance on mechanical properties. The MEA NiCoCr shows greater strength and ductility trade-off than any other binary, ternary, quaternary alloys or even quinary HEA alloys. With increasing interest in its potential application, the radiation response of MEA NiCoCr has been studied. Unfortunately, MEA NiCoCr exhibits abysmal performance under elevated temperature irradiation. The total swelling value in NiCoCr shows more than one order magnitude higher than other HEA alloys [15].

* Corresponding authors.
E-mail address: lmwang@umich.edu (L. Wang).
[1] Current address: Horia Hulubei National Institute for Physics and Nuclear Engineering, P.O.B. MG-6, 077125 Magurele, Romania.

https://doi.org/10.1016/j.jnucmat.2021.153316
0022-3115/

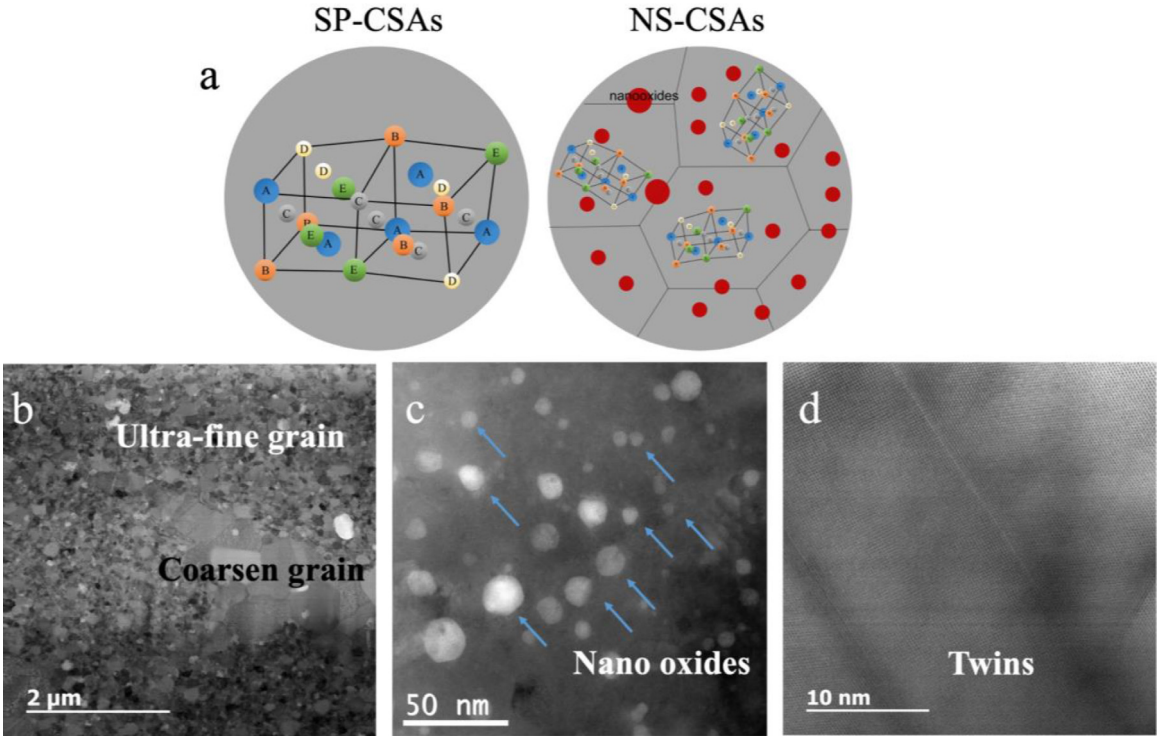

Fig. 1. (a) Schematics of the SP-CSAs and the design concept of the NS-CSAs; (b) STEM-BF image of NS-NiCoCr exhibiting bimodal grain structures; (c) HAADF image accentuating Y and Hf rich clusters on the basis of atomic-number contrast; (d) STEM-BF image showing the twins in NS-NiCoCr.

To take advantage of the promising mechanical properties of NiCoCr, simultaneously improving its radiation resistance behavior is necessary. There's a favorite way to improve radiation resistance behavior in alloys by introducing structural complexities, such as secondary phase or boundaries. The success of this approach has been demonstrated in oxide-dispersion-strengthened (ODS) steels [16–19], nano-grained polycrystalline alloys [20,21]. Therefore, nanostructured NiCoCr (termed NS-NiCoCr) enhanced by high-density nanooxides and grain boundaries is presented herein. Transmission electron microscopy (TEM) characterizations and nanoindentation tests show that the radiation resistance behavior of NS-NiCoCr is much better than single-phase medium entropy alloy NiCoCr, even better than single-phase high entropy alloy NiCoFeCrMn.

We want to emphasis that, the concept of combining compositional complexity with microstructural inhomogeneity is an advanced design principle, suitable for engineering other SP-CSAs. We aim to combine compositional complexity and structural complexity in one alloy, and controllably create the nanostructures for enhancing radiation resistance behaviour in fcc-type SP-CSAs, the new system is termed nanostructured concentrated solid solution alloys (NS-CSAs). Fig. 1 (a) show the schematics of the design concept for SP-CSAs and NS-CSAs, respectively. Such conceptual design enables us not only to enhance radiation resistance but also to maintain a promising strength-ductility combination. The compressive strength of the samples was tested at room temperature. The average yield strength and elongation of four tested samples are 1770 MPa and 9.985%. We have successfully designed a series NS-CSAs, the result of NS-NiCoCr is presented here to show the potential of improvement. The results on other NS-CSAs will be reported in follow.

2. Experiments

In this work, the nominal composition of the NS-NiCoCr alloy is NiCoCr-1.2Hf-1.5Y_2O_3. Elemental powders of Ni, Co, Cr, Hf and Y_2O_3 with >99.8% purity were processed by MA. MA was performed in planetary ball milling with a speed of 350 rpm. The ball-to-powder ratio is 10:1. And the ball-mill period is 60 h. The ball milled powders were subsequently consolidated by SPS technology at 1050 °C for 8 min. The sintering was performed in vacuum at a constant pressure of 50 MPa. The obtained alloy was then annealed at 850 °C for 24 hours, sequentially cooled down in the air. To better understand the effects of nanostructures, a single-phase NiCoCr (SP-NiCoCr) was also studied as a reference. The SP-NiCoCr was prepared using the arc-melting method at Oak Ridge National Laboratory [22].

Before ion irradiation, all samples were chemical-mechanically polished to get a mirror like surface. The ion irradiation experiments were conducted at Ion Beam Materials Lab (IBML) at the University of Tennessee, Knoxville [23]. Both SP-NiCoCr and NS-NiCoCr were irradiated with 3 MeV Ni^{2+} ions up to 5×10^{16} /cm^2 fluence at 580 °C. The flux was controlled at 2.8×10^{12} ions/cm^2s. A defocused beam was wobbled to achieve uniform irradiation. Stopping and range of ions in matter program (SRIM-2013) was used to predict the displacements per atom (dpa) and implanted ion concentration along the implantation depth. The prediction was conducted in full cascade mode with a displacement threshold energy of 40 eV [24]. According to the results shown in Fig. 2, the peak dose is about ~130 dpa with a dose rate of $\sim 7.3 \times 10^{-13}$ dpa/s. We also predicted the dpa value with SRIM-2013 code in quick Kinchin-pease mode, and the corresponding peak dose is about 64 dpa. Cross-sectional TEM samples were all prepared by focused ion beam (FIB) lift-out method on a FEI Helios Nanolab workstation. Sequentially, a "flash-polishing" technique was used to remove the FIB-induced damages and further thinned the FIB foil [25]. Scanning TEM (STEM) was employed for charactering microstructures using a double Cs-corrected JEOL 3100R05 at 300 keV. Atom probe tomography (APT) was carried out for analysing the compositional changes of nanooxides before and after irradiation. APT experiments were conducted using a CAMECA LEAP 4000X HR system. The APT specimens were running in laser mode

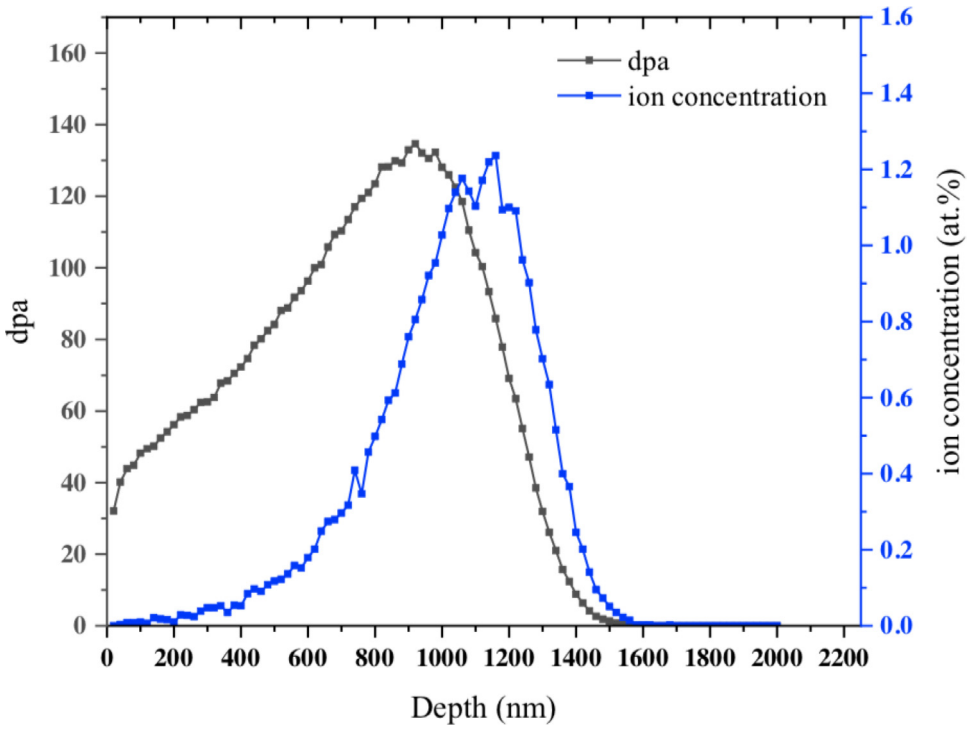

Fig. 2. Depth profiles of displacement per atom (dpa) and induced Ni ion concentration predicted by SRIM code (full cascade) for NS-NiCoCr irradiated with 3 MeV Ni^{2+} ions to a fluence of 5×10^{16} cm^{-2}.

at 30 K with a detection rate of 0.004 atom per pulse and a 40 pJ laser energy. The initial pulse repetition rate was set at 125 kHz in order to capture the heavy Hf ion. Once the APT specimen potential reached 5000 V, the pulse repetition rate was increased to 200 kHz. About 30 to 100 million ions were acquired for each APT specimen. Normal lift-out and sharpening procedures were followed to prepare the needle-shaped APT specimens. For both raw and 60 dpa samples, two APT specimens were prepared and analysed. To understand the mechanical changes of studied alloys before and after irradiation, nanoindentation was performed at room temperature using a Bruker Hystron TI950 Triboindenter at a constant $\dot{P}/P$=0.05 s^{-1}. The nanoindentation was used a spherical sapphire indenter with a diameter of 200 μm. All the samples were tested with a load control mode with the maximum load of 5000 μN and 8000 μN.

3. Results

The typical polycrystalline structure of NS-NiCoCr characterized by STEM Bright-field (BF) mode consists of an fcc structure with a bimodal grain size distribution as shown in Fig. 1(b). The coarse grains are usually larger than 1μm, while the fine grains are normally smaller than 200 nm. The inhomogeneous temperature gradient during SPS heating contributes to the particular bimodal grain distribution. Similar heterogeneous structures have been observed in SPSed ODS steel, previously [26,27]. Interestingly, this specific microstructure can significantly improve strength and ductility trade-off of the SPSed alloy according to the previous results [27]. By alloying with Hf and Y_2O_3 additions, we successfully introduced high-density nanooxides in the NiCoCr-base alloy. We broadly characterized the nanooxide distributions in the interior of nano grains, as shown in Fig. 1(c), with high angle annular dark field (HAADF) imaging technique. Nanooxides are shown as white dots in HAADF image because of the heavier element Hf and Y contained, which makes them higher mass compared to that of the NiCoCr matrix. The average diameter <d> of nanooxides is about ~6.9 nm with a number density <N> of 2×10^{22} $/m^3$. Besides of nanooxides and nano grains, a third structural complexity behaved as nanotwins, has been observed in NS-NiCoCr as shown in Fig. 1(d). According to a recent study, it is reasonable to believe that twins were formed during the MA and SPS processes, since the NiCoCr has a very low stacking fault energy and very high propensity for twining under low-level deformation. Actually, this preference to form nanotwins in early deformation range is exactly the reason why NiCoCr has better mechanical properties than other SP-CSAs [5,28–30]. Twin boundaries that separate a twin domain from parent crystal can effectively strengthen materials by impeding dislocation motion, and increase the ductility and work hardening capability of twinned metallic materials [31]. This result simultaneously indicates the NS-NiCoCr has similar deformation mechanisms with SP-NiCoCr. Furthermore, our previous result confirms that the incoherent edge of twin boundaries may also act as extra defect sinks for absorbing both irradiation-induced vacancies and interstitials, sequentially lowing the residual defect concentration in alloy matrix [32].

To understand the enhancement of the properties of NS-NiCoCr, the atomic structures of nanooxides were further characterized by high resolution STEM-BF, HAADF and electron dispersion spectrum (EDS) line scanning (Fig. 3). Fig. 3(a) shows high-resolution STEM-BF and HAADF images of a typical oxide, the diameter of this nanooxide is only 3.5 nm. The inter-planer spacing and angles are reasonably consistent with the defected fluorite-structured $Y_2Hf_2O_7$ [34]. Incident electron is parallel to the [010], with two atomic planes are ($\bar{2}$00) and (200). This nanooxide clearly displays faceted interfaces along low-index planes of the matrix, the shape of this nanooxide is shown in a near regular octagon. In Fig. 3(b), the white contrast of the dots in the lattice indicates the heavier element enriched in nanooxide as shown in HAADF image, such as Y and Hf. EDS line scanning result clearly shows that the nanooxide is enriched with yttrium, hafnium and oxygen elements as shown in Fig. 3(b). Details of the elemental composition of nanooxides before and after irradiation are characterized by APT, which

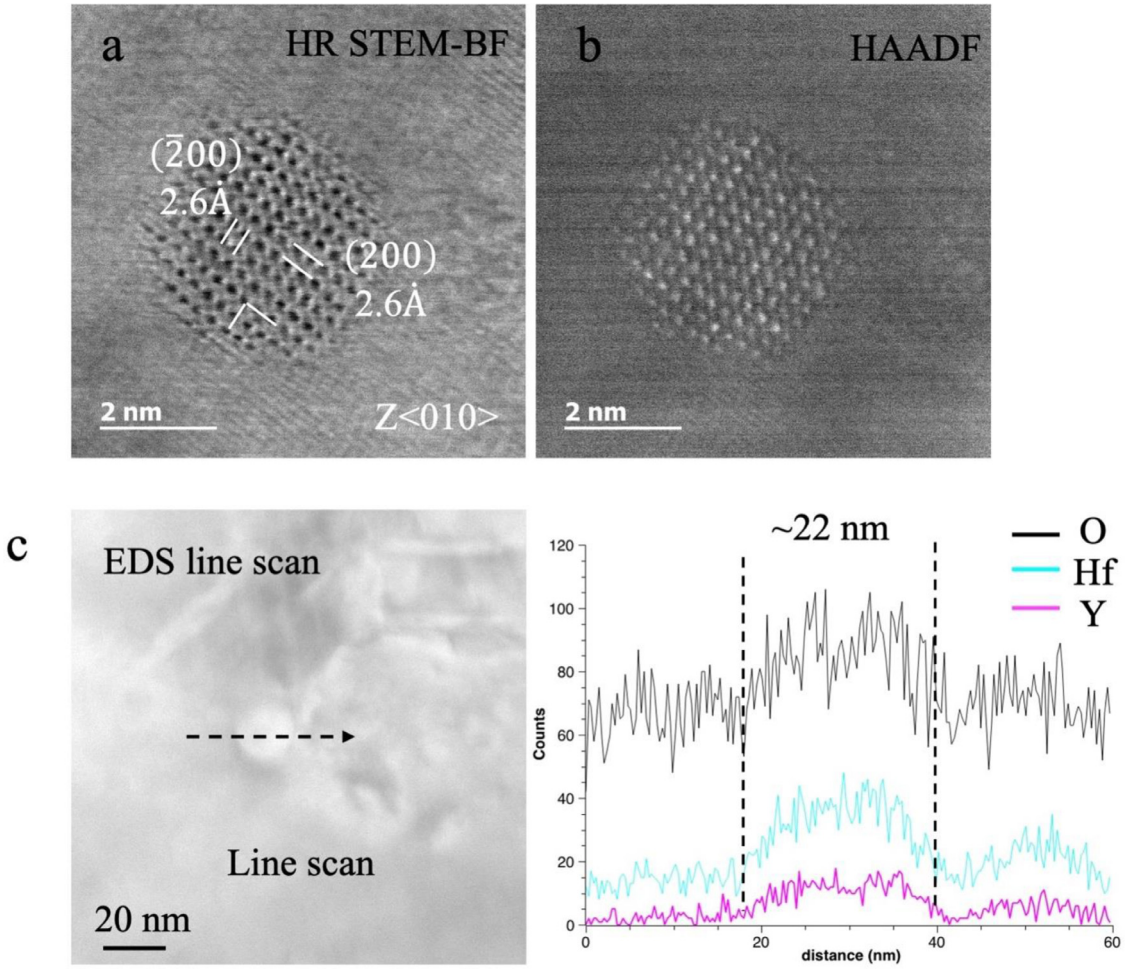

Fig. 3. (a) High resolution STEM-BF and HAADF images showing the pyrochlore structured $Y_2Hf_2O_7$; (b) HAADF image and (c) EDS line scan result showing the nanooxide enriched with Y, Hf and O.

will be shown in below. This result is consistent with the TEM observations and the results reported from other ODS alloys [35].

The NS-NiCoCr exhibits excellent swelling resistance as compared to SP-NiCoCr. As shown in Figs. 4 (a) and (b), ex-situ 3 MeV Ni^+ ion irradiation of SP-NiCoCr to 5×10^{16} /cm^2 fluence (peak dose is ~130 dpa) at 580 °C leads to a significant void swelling, whereas NC-NiCoCr irradiated under the same condition has no observable voids. Both STEM images in Fig. 4 (a) and (b) present the panoramic cross-sectional views of the alloys after irradiation, the sample surfaces are on the top, and the depth is marked on the side. Clearly, large voids are formed in entire irradiation damage zone in SP-NiCoCr, leading a significant overall swelling of ~9.34%. In high temperature irradiated SP-CSAs, while voids are the result of three-dimensional agglomeration of irradiation-induced vacancies, dislocation loops and network dislocations are often the most typical defects due to the agglomeration of irradiation-induced interstitials [36]. Furthermore, it is known that, in fcc structure alloys, faulted loops could transform into unfaulted/perfect loops through interstitial atom absorption on the {111} planes according to this reaction [33]:

$$(a/3) < 111 > + (a/6) < 112 > = (a/2) < 110 > \quad (1)$$

In NiCoCr, the lower stacking fault energy leads this transformation easier. As we know that the unfaulted/perfect loops are mobile and easily to aggregate together to form dislocation lines and dislocation complex, which will lead the static swelling stage of the alloys. Fig. 4(a) was taken near the [110] zone axis to maximize the visibility of all the irradiation-induced features [37]. High density of network dislocations and dislocation loops are found in SP-NiCoCr after irradiation. These features could result in severe degradation of mechanical properties of structural materials, such as irradiation induced hardening and embrittlement. On the contrary, no detectable dislocation loops can be found in NS-NiCoCr under the same irradiation condition, indicating that either most of the survived interstitials have been annihilated in the matrix, or the size of dislocation loops is too small to observe. Nanoindentation results present that NS-NiCoCr has no apparent hardening after irradiation, as shown in Fig. 4(c), indicating that there are no strong hardening sources formed. Usually, dislocation loops and voids are considered as the strong hardening source for alloys, therefore, the nanoindentation results support TEM observations that no detectable voids and dislocation loops were formed in NS-NiCoCr after high temperature irradiation. In conclusion, NS-NiCoCr has an extraordinary swelling resistance behavior, simultaneously has a promising hardening resistance property.

The fine dispersion of nanooxides and high-density grain boundaries are believed to provide resistance to irradiation damage. Therefore, understanding their stabilities after irradiation is very important. Any changes in nanooxides and grains (including size, density, chemistry and crystal structure) will have implications on mechanical properties, irradiation defect evolution and material performance. The NS-NiCoCr shows an exceptionally stability against heavy ion irradiation. No detectable grain growth is observed after 3 MeV Ni^+ irradiation to a fluence of 5×10^{16}/cm^2

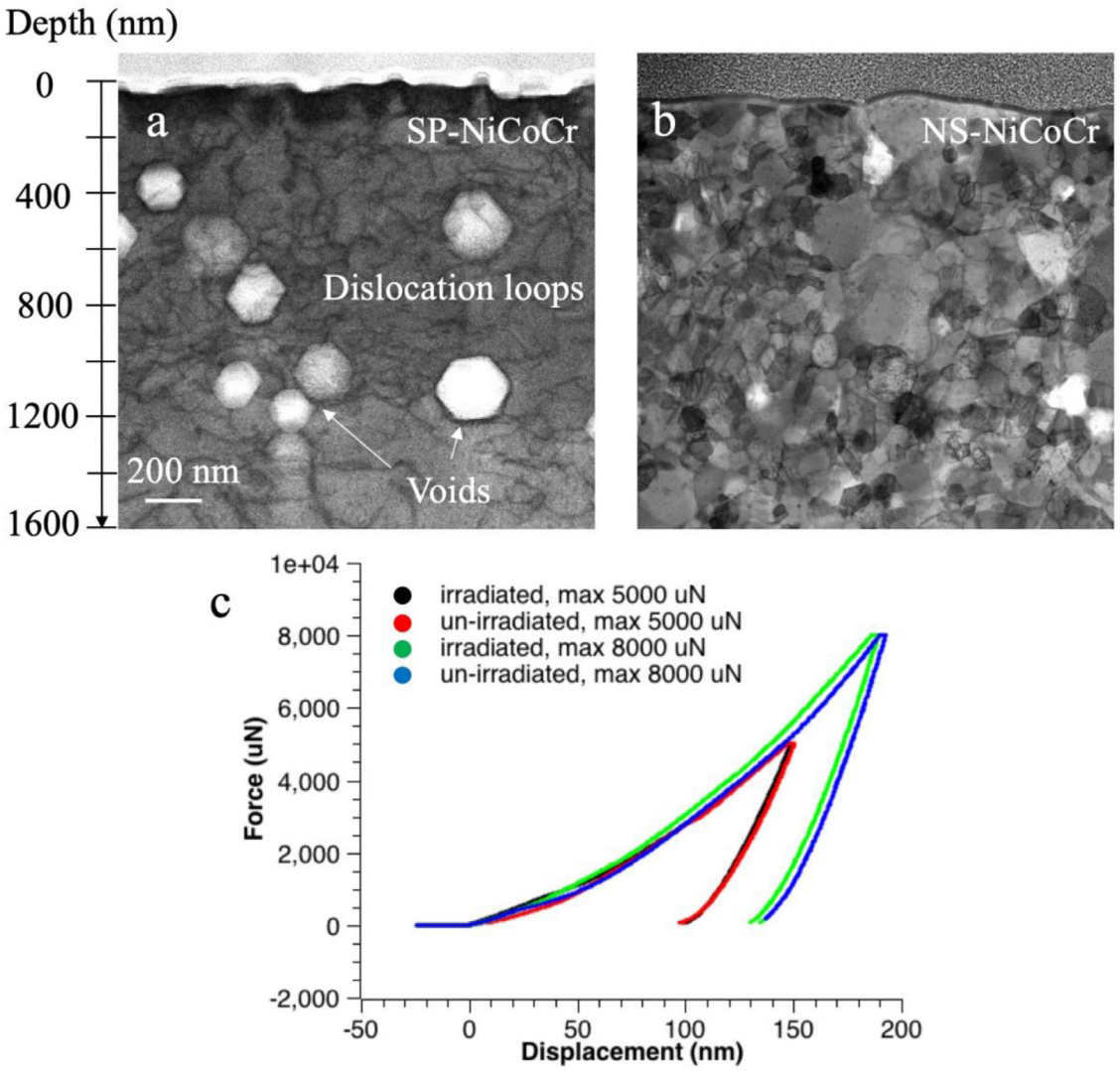

Fig. 4. Cross-sectional STEM images of (a) SP-NiCoCr and (b) NS-NiCoCr after irradiation to show the void and dislocation distributions. (c) Load-unload curves of an un-irradiated and an irradiated NS-NiCoCr showing that no serious hardening occurred after irradiation.

at 580 °C. In addition, only slight oxide shrinking is observed in NS-NiCoCr after irradiation. More details can be found in Fig. 5. Fig. 5(a) shows the cross-sectional STEM image of NS-NiCoCr after irradiation. The white rectangle shows the region irradiated to 60 dpa. The enlarged image clearly shows that high density of nanooxides homogenously dispersed in the matrix, while all the nanooxides successfully kept their crystalline structures after 60 dpa irradiation at 580°C since the misfit moiré fringes observed. Comparing to the oxide distribution before irradiation ($<d> = 6.95$ nm, $<N> = 2 \times 10^{22}$ /m^3), the average size of nanooxides slightly decreased with a $<d> = 5.9$ nm, and the number density increased to $<N> = 7 \times 10^{22}$ /m^3 after 60 dpa irradiation at 580 °C. Oxide size distribution before and after 60 dpa irradiation in NS-NiCoCr is shown in Fig. 5(c). Clearly, in irradiated NS-NiCoCr, the peak distribution slightly towards to left, indicating that more amounts of smaller nanooxides existing after irradiation. The shrinkage of nanoparticles in other ODS alloys have been reported many times. Allen, et al. and Chen et al. both observe the decreasing nanoparticles size with increasing dose in ODS steel [38,39]. The stability of precipitates in alloys after irradiation has been widely studied and the mechanism can be concluded as the competition between collision cascade and radiation enhanced diffusion. The growth and the shrinkage highly depend on the irradiation temperature and dose. G. Yeli et. al., have done an excellent job on understanding the behavior of γ' precipitate in multi-component $FeCoNiCrTi_{0.2}$ alloy after irradiation. The obtained results are similar to this study, and the underlying mechanism can also explain the nanooxides shrinkage effect in ODS NiCoCr alloy [40]. It is worth noting that, although the size of original nanoxides in NS-NiCoCr decreases slightly during the irradiation, the increased density of more uniform (narrower size distribution) nanooxides is highly desirable as such modified (towards self-assemble) stable precipices can actually provide more trapping sites for point defects, which can further improve radiation tolerance [26].

The changes of nanooxide chemistry have been studied by APT as shown in Fig. 6 (a). Since the nanooxide are enriched with Y, we used Y iso-concentration surface at 5 at. % to define the dimension of the nanoxide and locate their positions in the APT reconstruction. As shown in Fig. 6(a), the Y iso-concentration surface is colored in blue and the matrix elements are colored in green. Based on the APT analyses, the nanooxide number density in the ODS NiCoCr sample is 6.26×10^4/mm^3 before irradiation, and 7.01×10^4 /mm^3 after irradiation. The average diameter of nanooxides are 10.79 nm and 8.08 nm before and after irradiation, respectively. The difference between TEM and APT statistics may come from relatively larger volume being sampled by TEM, and also the different methods in defining the dimension

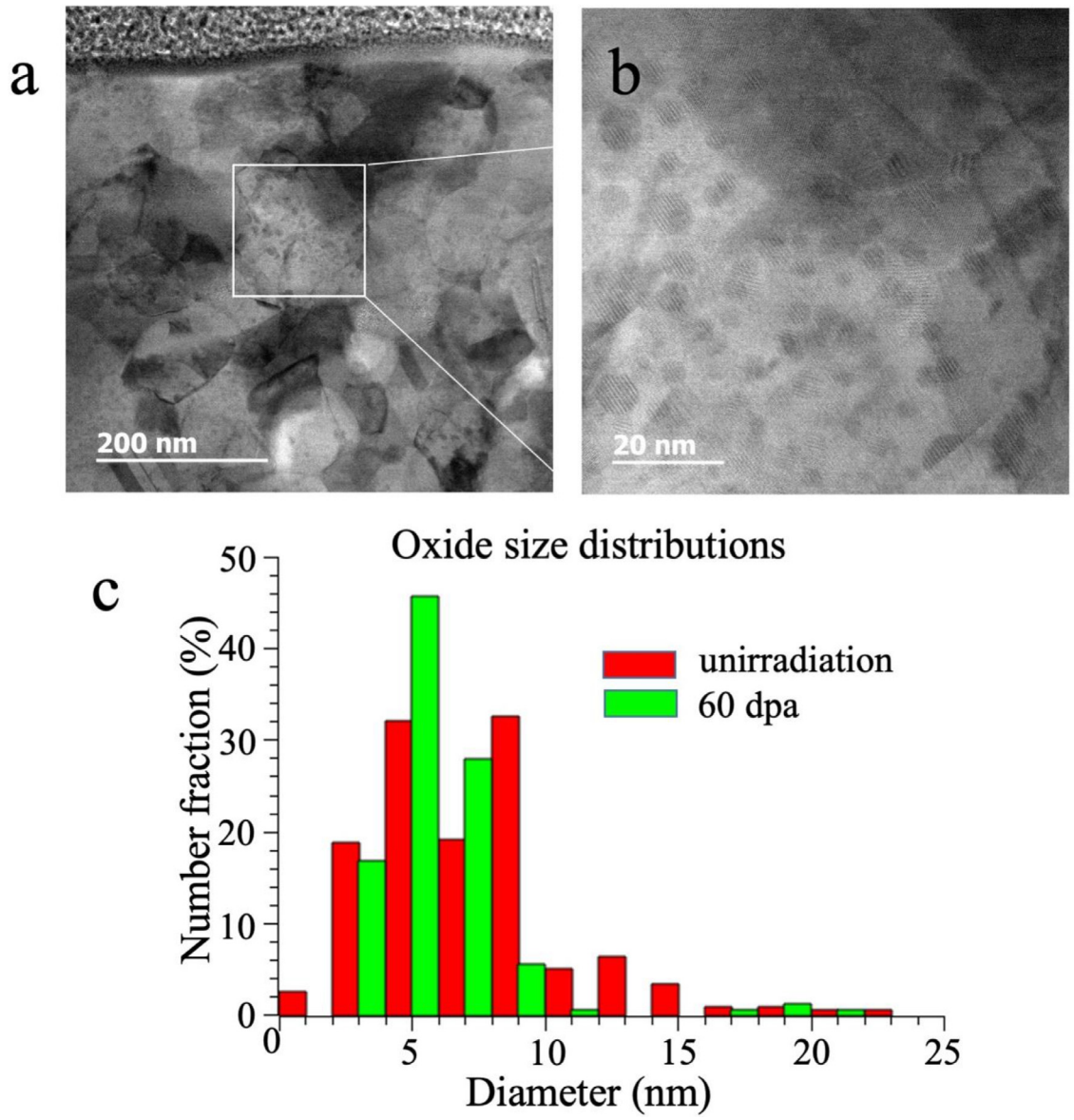

Fig. 5. (a) STEM-BF image of NS-NiCoCr after irradiation showing the stable of grains and nanooxides; (b) enlarged STEM-BF image of rectangle in (a); (c) size distributions of nanooxides before and after 60 dpa irradiation.

of the nanooxide in APT. Typical 1D composition profiles across the boundaries of nanooxides were obtained based on the APT reconstructions (Fig. 6b). These profiles were calculated based on atom numbers in cylindrical regions of interest passing through the oxide with a 8 nm cylinder dimeter and a 2 nm bin size. The results show that, in non-irradiated samples, the Ni, Co, Cr concentration will gets very close to 0% in the center of the oxide particle; while in the irradiated samples, for oxide particles in similar sizes to the non-irradiated samples, the Ni, Co, Cr concentration cannot get to 0% (~5 at.%), and the oxide/matrix boundary becomes wider, indicating that the radiation may lead to element intermixing of the matrix with the nanooxide.

4. Discussion

Several strategies can be used to stabilize the grain boundaries under thermal annealing and energetic particle irradiation. Recent research successfully defeats grain growth thermodynamically by introducing La atoms at grain boundaries [20]. On the contrary, a kinetic strategy has been conducted in this study by pining the grain boundaries using nanooxides. The high density of nanooxides can counteract the driving pressure from the curvature of the grain boundary, and sequentially impede the grain growth [41]. Generally, it is believed that structural complexities/inhomogeneity, such as grain boundaries, dislocations, interfaces between the matrix and precipitates, can act as preferential sinks for annihilating irradiation-induced vacancies and interstitials [42]. It is worth noting that, grain boundaries have been considered as neutral (unbiased) sinks that have no preference for capturing interstitials or vacancies [42]. However, the pyrochlore structured $Y_2Hf_2O_7$ nanooxide is semi-coherent with the Fe matrix. Therefore, they could be considered as the variable bias sinks to act as recombination centers to annihilate interstitials and vacancies [42]. Kinetic rate theory has been conducted to quantitatively predict the sink strengths of grain boundaries and nanooxide/matrix interfaces [43]. The sink strength of the nanooxide/matrix interfaces is given by $S_o = 4\pi N(0.3A^{1/2})$, where N is the number density of the nanooxides, A is the surface area of the nanooxides, $A = 4\pi r^2$, r is the average radius of the nanooxides. Considering the continuous changes of nanooxide size and density during the irradia-

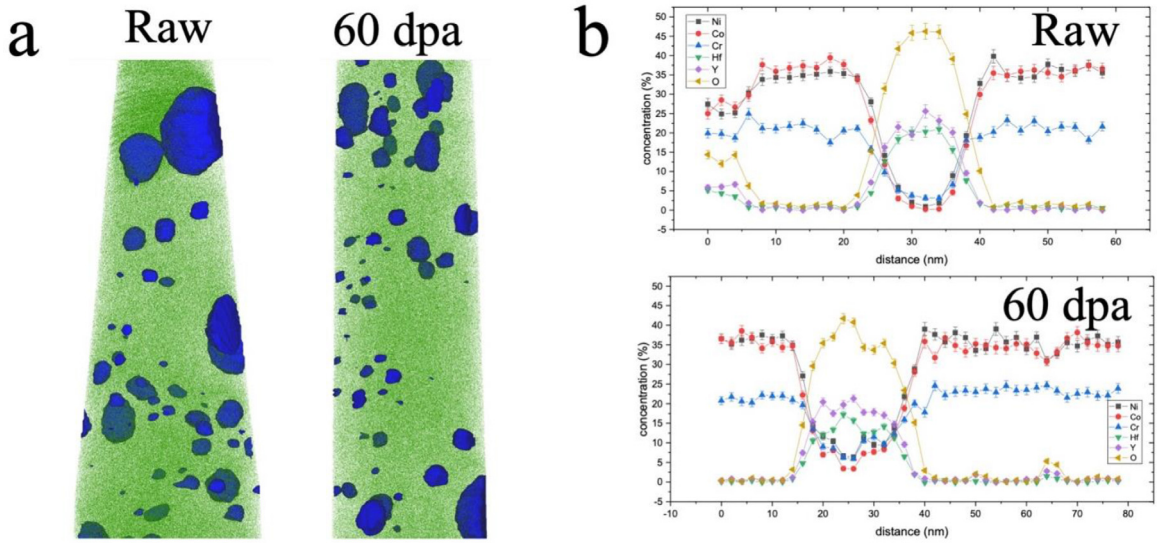

Fig. 6. (a) Atom probe tomography three-dimensional reconstructions from the analysis of two specimen from un-irradiated and irradiated NS-NiCoCr; (b) typical 1D composition profiles across boundaries of nanooxides from un-irradiated and irradiated NS-NiCoCr.

tion, we used the final distribution of the nanooxides (r = 2.95 nm, N' =7 × 10^{22} /m^3) in the NiCoCr matrix, which obtains S_o = 2.75 × $10^{15}m^{-2}$. The sink strength of grain boundaries is given by $S_b = 60/D^2$, where D is the average grain diameter. Neglecting the weak sink strength from coarse grains, the S_b for fine grains is 1.5 × $10^{15}m^{-2}$. These data indicate that both grain boundaries and nanooxides play a significant role in suppressing the formation of voids and dislocation loops. The results are in agreement with previous experimental and simulation results [20,26,44].

5. Conclusions

In conclusion, we have studied the radiation tolerance of a newly developed NS-NiCoCr alloy with promising mechanical properties. Compared to the poor swelling resistance of SP-NiCoCr, the NS-NiCoCr demonstrated a superb radiation resistance showing no neither and dislocation loop after a severe ion irradiation condition. Furthermore, high-density dispersed nanooxides kept their crystalline structure and stabilized the grain boundaries during the high temperature ion irradiation. High sink strength from high density nanooxides and grain boundaries contribute to this excellent radiation tolerance in NS-NiCoCr. Our findings on the high radiation tolerance of NS-NiCoCr have clearly shown the significant property enhancement by taking advances of both compositional complexity and microstructural inhomogeneity, and provide insights for developing next generation of radiation-tolerant medium/high entropy alloys by introducing additional structural complexities.

Declaration of Competing Interest

The authors declare that they have no known competing financial interests or personal relationships that could have appeared to influence the work reported in this paper.

The authors declare the following financial interests/personal relationships which may be considered as potential competing interests:

CRediT authorship contribution statement

Chenyang Lu: Conceptualization, Methodology, Investigation, Writing – original draft. **Mingyang Li:** Resources. **Pengyuan Xiu:** Investigation. **Xing Wang:** Investigation. **Gihan Velişa:** Investigation. **Li Jiang:** Investigation. **Karren L. More:** Visualization, Supervision. **Jonathan D. Poplawsky:** Investigation. **Yongqin Chang:** Resources, Supervision. **Yanwen Zhang:** Funding acquisition, Resources, Supervision. **Lumin Wang:** Funding acquisition, Resources, Writing – review & editing, Supervision.

Acknowledgements

This work was supported as part of the Energy Dissipation to Defect Evolution (EDDE) Center, an Energy Frontier Research Center funded by the US Department of Energy, Office of Science, Basic Energy Sciences. Ion beam work was performed at the UT–ORNL Ion Beam Materials Laboratory located on the campus of the University of Tennessee–Knoxville. The TEM analysis was conducted in the Michigan Center for Material Characterization of the University of Michigan.

References

[1] J.W. Yeh, S.K. Chen, S.J. Lin, J.Y. Gan, T.S. Chin, T.T. Shun, C.H. Tsau, S.Y. Chang, Nanostructured high-entropy alloys with multiple principal elements: novel alloy design concepts and outcomes, Adv. Eng. Mater. 6 (2004) 299–303.
[2] Y. Zhang, T.T. Zuo, Z. Tang, M.C. Gao, K.A. Dahmen, P.K. Liaw, Z.H. Lu, Microstructures and properties of high-entropy alloys, Prog. Mater. Sci. 61 (2013) 1–93.
[3] O.N. Senkov, G.B. Wilks, J.M. Scott, D.B. Miracle, Mechanical properties of Nb25Mo25Ta25W25 and V20Nb20Mo20Ta20W20 refractory high entropy alloys, Intermetallics 19 (2011) 698–706.
[4] Z.M. Li, Y.Deng K.G.Pradeep, C.C.Tasan D.Raabe, Metastable high-entropy dual-phase alloys overcome the strength-ductility trade-off, Nature 534 (7606) (2016) 227–230.
[5] B. Gludovatz, A. Hohenwarter, D. Catoor, E.H. Chang, E.P. George, R.O. Ritchie, A fracture-resistant high-entropy alloy for cryogenic applications, Science 345 (2014) 1153–1158.
[6] F. Otto, Y. Yang, H. Bei, E.P. George, Relative effects of enthalpy and entropy on the phase stability of equiatomic high-entropy alloys, Acta Mater. 61 (7) (2013) 2628–2638.
[7] N.A.P.K. Kumar, C. Li, K.J. Leonard, H. Bei, S.J. Zinkle, Microstructural stability and mechanical behavior of FeNiMnCr high entropy alloy under ion irradiation, Acta Mater. 113 (2016) 230–244.
[8] C.Y. Lu, L.L. Niu, N.J. Chen, K. Jin, N.Y. T, P.Y. Xiu, Y.W. Zhang, F. Gao, H.B. Bei, S. Shi, M.R. He, I.M. Robertson, W.J. Weber, L.M. Wang, Enhancing radiation tolerance by controlling defect mobility and migration pathways in multicomponent single-phase alloys, Nat. Commun. 7 (2016) 13564.
[9] T.N. Yang, C.Y. Lu, G. Velisa, K. Jin, P.Y. Xiu, Y.W Zhang, H.B. Bei, L.M. Wang, Influence of irradiation temperature on void swelling in NiCoFeCrMn and NiCoFeCrPd, Scr. Mater. 158 (2019) 57–61.

[10] C.Y. Lu, T.N. Yang, K. Jin, G.H. Velisa, P.Y. Xiu, M. Song, Q. Peng, F. Gao, Y.W. Zhang, H.B. Bei, W.J. Weber, L.M. Wang, Enhanced void swelling in NiCoFeCrPd high-entropy alloy by indentation-induced dislocations, Mater. Res. Lett. 6 (10) (2018) 584–591.
[11] T.F. Yang, S.Q. Xia, W. Guo, R. Hu, J.D. Poplawsky, G. Sha, Y. Fang, Z.F. Yan, C.X. Wang, C.Y. Li, Y. Zhang, S.J. Zinkle, Y.G. Wang, Effects of temperature on the irradiation responses of Al0.1CoCrFeNi high entropy alloy, Scr. Mater. 144 (2018) 31–35.
[12] Y.P. Lu, H.F. Huang, X.Z. Gao, C.L. Ren, J. Gao, H.Z. Zhang, S.J. Zheng, Q.Q. Jin, Y.H. Zhao, C.Y. Lu, T.M. Wang, T.J. Li, A promising new class of irradiation tolerant materials: Ti2ZrHfV0.5Mo0.2 high-entropy alloy, J. Mater. Sci. Technol. 35 (3) (2019) 369–373.
[13] A. Barashev, Y. Osetsky, H.B. Bei, C.Y. Lu, L.M. Wang, Y.W. Zhang, Chemically-biased diffusion and segregation impede void growth in irradiated Ni-Fe alloys, Curr. Opin. Solid State Mater. Sci. 23 (2) (2019) 92–100.
[14] Y.N. Osetsky, L.K. Béland, A.V. Barashev, Y.W. Zhang, On the existence and origin of sluggish diffusion in chemically disordered concentrated alloys, Curr. Opin. Solid State Mater. Sci. 22 (3) (2018) 65–74.
[15] K. Jin, C.Y. Lu, L.M. Wang, J. Qu, W.J. Weber, Y.W. Zhang, H.B. Bei, Effects of compositional complexity on the ion-irradiation induced swelling and hardening in Ni-containing equiatomic alloys, Scr. Mater. 119 (2016) 65–70.
[16] G.R. Odette, M.J. Alinger, B.D. Wirth, Recent developments in irradiation-resistant steels, Annu. Rev. Mater. Sci. 38 (1) (2008) 471–503.
[17] G.R. Odette, D.T. Hoelzer, Irradiation-tolerant nanostructured ferritic alloys: transforming helium from a liability to an asset, JOM 62 (2010) 84–92.
[18] C.Y. Lu, Z. Lu, R. Xie, C.M. Liu, L.M. Wang, Microstructure of HIPed and SPSed 9Cr-ODS steel and its effect on helium bubble formation, J. Nucl. Mater. 474 (2016) 65–75.
[19] A. Hirata, T. Fujita, Y.R. Wen, J.H. Schneibel, C.T. Liu, M.W. Chen, Atomic structure of nanoclusters in oxide-dispersion-strengthened steels, Nat. Mater. 10 (12) (2011) 922–926.
[20] C.C. Du, S.B. Jin, Y. Fang, J. Li, S.Y. Hu, T.T. Yang, Y. Zhang, J.Y. Huang, G. Sha, Y.G. Wang, Z.X. Shang, X.H. Zhang, B.R. Sun, S.W. Xin, T.D. Shen, Ultrastrong nanocrystalline steel with exceptional thermal stability and radiation tolerance, Nat. Commun. 9 (1) (2018) 5389.
[21] X.H. Zhang, K. Hattar, Y.X. Chen, L. Shao, J. Li, C. Sun, K.Y. Yu, N. Li, M.L. Taheri, H.Y. Wang, J. Wang, M. Nastasi, Radiation damage in nanostructured materials, Prog. Mater. Sci. 96 (2018) 217–321.
[22] K. Jin, S. Mu, K. An, W.D. Porter, G.D. Samolyuk, G.M. Stocks, H. Bei, Thermophysical properties of Ni-containing single-phase concentrated solid solution alloys, Mater. Des. 117 (2017) 185–192.
[23] Y. Zhang, M.L. Crespillo, H. Xue, K. Jin, C.H. Chen, C.L. Fontana, J.T. Graham, W.J. Weber, New ion beam materials laboratory for materials modification and irradiation effects research, Nucl. Inst. Method. Phys. Res., B. 338 (2014) 19–30.
[24] W.J. Weber, Y.W. Zhang, Predicting damage production in monoatomic and multi-elemental targets using stopping and range of ions in matter code: challenges and recommendations, Curr. Opin. Solid State Mater. Sci. 23 (4) (2019).
[25] C.Y. Lu, K. Jin, L.K. Beland, F.F. Zhang, T.N. Yang, L. Qiao, Y.W. Zhang, H.B. Bei, H.M. Christen, R.E. Stoller, L.M. Wang, Direct observation of defect range and evolution in ion-irradiated single crystalline Ni and Ni binary alloys, Sci. Rep. 6 (2016) 19994.
[26] C.Y. Lu, Z. Lu, X. Wang, R. Xie, Z.Y. Li, M. Higgins, C.M. Liu, F. Gao, L.M. Wang, Enhanced radiation-tolerant oxide dispersion strengthened steel and its microstructure evolution under Helium-implantation and Heavy-ion Irradiation, Sci. Rep. 7 (2017) 40343.
[27] X. Boulnat, D. Fabregue, M. Perez, M.H. Mathon, Y. De Carlan, High-temperature tensile properties of Nano-oxide dispersion strengthened ferritic steels produced by mechanical alloying and spark plasma sintering, Metall Mater Trans A Phys Metall Mater Sci 44 (6) (2013) 2461–2465.
[28] G. Laplanche, A. Kostka, C. Reinhart, J. Hunfeld, G. Eggeler, E.P. George, Reasons for the superior mechanical properties of medium-entropy CrCoNi compared to high-entropy CrMnFeCoNi, Acta Mater. 128 (2017) 292–303.
[29] J. Miao, C.E. Slone, T.M. Smith, C. Niu, H. Bei, M. Ghazisaeidi, G.M. Pharr, M.J. Mills, The evolution of the deformation substructure in a Ni-Co-Cr equiatomic solid solution alloy, Acta Mater. 132 (2017) 35–48.
[30] S.J. Zhao, Y. Osetsky, G.M. Stocks, Y.W. Zhang, Local-environment dependence of stacking fault energies in concentrated solid-solution alloys, NPJ Comput 5 (1) (2019).
[31] J. Wang, X.H. Zhang, Twinning effects on strength and plasticity of metallic materials, MRS Bull. 41 (4) (2016) 274–281.
[32] C.Y. Lu, T.N. Yang, K. Jin, G. Velisa, P.Y. Xiu, Q. Peng, F. Gao, Y.W. Zhang, H.B. Bei, W.J. Weber, L.M. Wang, Irradiation effects of medium-entropy alloy NiCoCr with and without pre-indentation, J. Nucl. Mater. 524 (2019) 60–66.
[33] I.M. Neklyudov, V.N. Voyevodin, Features of structure-phase transformations and segregation processes under irradiation of austenitic and ferritic-martensitic steels, J. Nucl. Mater. 212 (1994) 39–44.
[34] H. Oka, M. Watanabe, N. Hashimoto, S. Ohnuki, S. Yamashita, S. Ohtsuka, Morphology of oxide particles in ODS austenitic stainless steel, J. Nucl. Mater. 442 (1-3) (2013) S164–S168.
[35] Y.N. Huang, H.T. Zhang, M.A. Auger, Z.L. Hong, H.P. Ning, M.J. Gorley, P.S. Grant, M.J. Reece, H.X. Yan, S.G. Roberts, Microstructural comparison of effects of hafnium and titanium additions in spark-plasma-sintered Fe-based oxide-dispersion strengthened alloys, J. Nucl. Mater. 487 (2017) 433–442.
[36] S.J. Zinkle, L.L. Snead, Designing Radiation Resistance in Materials for Fusion Energy, Annu. Rev. Mater. Sci. 44 (1) (2014) 241–267.
[37] C.M. Parish, K.G. Field, A.G. Certain, J.P. Wharry, Application of STEM characterization for investigating radiation effects in BCC Fe-based alloys, J. Mater. Res. 30 (9) (2015) 1275–1289.
[38] T.R. Allen, J. Gan, J.I. Cole, M.K. Miller, J.T. Busby, S. Shutthanandan, S. Thevuthasan, Radiation response of a 9 chromium oxide dispersion strengthened steel to heavy ion irradiation, J. Nucl. Mater. 375 (1) (2008) 26–37.
[39] T.Y. Chen, J.G. Gigax, L. Price, D. Chen, S. Ukai, E. Aydogan, S.A. Maloy, F.A. Garner, L. Shao, Temperature dependent dispersoid stability in ion-irradiated ferritic-martensitic dual-phase oxide-dispersion-strengthened alloy: Coherent interfaces vs. incoherent interfaces, Acta Mater. 116 (2016) 29–42.
[40] G. Yeli, D. Chen, K. Yabuuchi, A. Kimura, S.F. Liu, W.T. Lin, Y.L. Zhao, S.J. Zhao, J.-J. Kai, The stability of γ' precipitates in a multi-component FeCoNiCrTi0.2 alloy under elevated-temperature irradiation, J. Nucl. Mater. 540 (2020) 152364.
[41] C.S. Zener, Grains, phases and interfaces: an interpretation of microstructure, Trans. AIME. 175 (1948) 15–51.
[42] G.S. Was, Fundamentals of radiation materials science: metals and alloys, (2007).
[43] L.K. Mansur, Theory and experimental background on dimensional changes in irradiated alloys, J. Nucl. Mater. 216 (1994) 97–123.
[44] X.M. Bai, A.F. Voter, R.G. Hoagland, M. Nastasi, B.P. Uberuaga, Efficient annealing of radiation damage near grain boundaries via interstitial emission, Science 327 (2010) 1631–1634.